Arch. Mech., 43, 4, pp. 499–517, Warszawa 1991

Behavior of rock salt in uniaxial compression at medium and high strain rates

J. R. KLEPACZKO (METZ), G. GARY and P. BARBERIS (PALAISEAU)

THIS PAPER presents results of experiments on the rock salt. The overall objective of this research was to determine the crushing stress, crushing strain and crushing energy over a wide spectrum of strain rates, $3 \times 10^{-5}\,s^{-1} \leq \dot{\varepsilon} \lesssim 4 \times 10^{2}\,s^{-1}$. Three experimental setups have been used to cover the whole spectrum: two testing machines and a split Hopkinson pressure bar. It has appeared that the rate-dependence of the three quantities studied is a highly complicated function of strain rate. At low strain rates, $\dot{\varepsilon} < 10^{-4}\,s^{-1}$, plastic flow dominates. Within the low and medium strain rates $10^{-4}\,s^{-1} \leq \dot{\varepsilon} \leq 1\,s^{-1}$ a more intense microcracking is superimposed on plastic flow causing rate-dependent damage. It has been found that the rate-dependent damage causes a negative rate sensitivity of crushing stress, crushing strain and crushing energy, a very practical observation. The last part of the paper concentrates on general discussion of one-dimensional constitutive relations which include intrinsic rate effects and rate-dependent damage. Finally, the region of the highest strain rate is discussed from the point of view of pressure dependence and inertia of microcracking. In all cases the quantitative estimations of the rate sensitivities are provided.

1. Introduction

IN RECENT YEARS mechanical behavior of halite, in the pure form or as the natural rock, has attracted a lot of attention. This has been caused by the rock salt relevance in connection with nuclear waste repositories. Long-term repository performance must be predicted and it provides an engineering challenge. It is important to collect for this purpose as many as possible experimental data on mechanical properties of halite tested in the form of single crystals as well as polycrystalline natural or artificial material. A lot of effort has been devoted so far to creep tests at different temperatures, for both irradiated and non-irradiated halite. Since the long-term repository performance must be rather predicted than determined directly from the in-situ behavior, a valid predictive model or a set of models must be developed. Those models must represent physical phenomena like strain hardening, microstructural evolution, effects of irradiation, effect of hydrostatic pressure and, finally, temperature and rate sensivity.

Because during plastic deformation halite is highly rate sensitive, it has been decided to test the natural rock salt over a wide range of strain rates. Although relatively numerous literature is available on creep of halite and rock salt, very limited data can be found on mechanical behavior of those materials at medium and high strain rates.

It is important to mention that relatively ample literature exists on rate sensitivity of rocks tested at medium strain rates, for example early papers by SERDENGECTI and BOOZER [1], CHEATHAM [2], and at high strain rates HAKALEHTO [3], LINDHOLM *et al.* [4], CHRISTENSEN *et al.* [5] and PERKINS *et al.* [6].

Another type of dynamic test performed on rocks is high strain-rate impulse loading, for example GRADY and KIPP [7], and FORRESTAL *et al.* [8]. At those very high rates of loading description of dynamic damage and fragmentation is of great importance. Fracture

and fragmentation data for rocks obtained at high loading rates clearly demonstrate the rate dependence of fracture strength and fragment size [7].

The problems like rate sensitive damage and fragmentation along with dynamic fracture can be adressed for halite and natural rock salt. It is clear that question concerning all aspects of the influence of rate effects in mechanical behavior of halite and natural rock salt have not been extensively explored. Besides of practical importance of dynamics in the nuclear waste repositories, like the effects of earthquakes and explosions, it is necessary to compare mechanical behavior of this material with another kinds of rocks. Such studies are crucial in constitutive modeling. It is believed that the present study will provide a more rational approach to rate sensitivity and fragmentation of rock salt via interpretation and discussion of experimental evidence.

2. Quasi-static tests in compression

It is the purpose of this study to apply the unified stress-strain approach in determining crushing stress, crushing strain and crushing energy in uniaxial stress compression for the rock salt. It was intended to perform compression tests over the widest possible range of strain rates, quasi-static, medium and high. In order to complete the whole strain rate spectrum, several strain rates are usually applied. Part of the spectrum can be obtained using standard closed-loop testing machines. However, higher strain rates, usually in excess of $\dot{\varepsilon} = 1\,\mathrm{s}^{-1}$, can be obtained only with the aid of specially designed setups.

Since it is desirable to use always the same specimen geometry, designed for quasi-static as well as for impact testing, a short disc shape has been accepted. Rock salt specimens of initial diameter $d_0 = 36$ mm and initial height $l_0 = 40$ mm were used throughout the testing. For such specimen geometry the height to diameter ratio is equal $l_0/d_0 = 1.11$. This aspect ratio is a compromise between value of 2 recommended in quasi-static tests and value of $\sim 1/2$ recommended for impact tests with the split Hopkinson pressure bar, KOLSKY [9], DAVIES and HUNTER [10], MALINOWSKI and KLEPACZKO [11].

All specimens have been prepared from the salt mine in Alsace (France), Mines de Potasse d'Alsace (MDPA). More exact characterization of the storage sites in France has been published by BÉREST and NGUYEN MINH, [12]. First, the bars of salt were drilled out and next machined and cut to the final dimensions. Small flaws or cavities, if present, were filled with special cement. The faces of specimens were treated in the same way to assure parallelism better than 0.1 mm. Such procedure has eliminated random stress concentrators and diminished the scatter of experimental results. The largest grains of salt did not exceed the value of 10 mm. Thus, in the less favorable case, the specimen could contain about 10 grains. Between the grains a sediment was clearly visible.

Since the order of maximum crushing strain ε_f for the rock salt specimen described above, and tested in the quasi-static regime, is about 1×10^{-2}, it is important to have a high resolution of strain reading. The displacement U_f to crush the salt specimen is about 0.4 mm and, consequently, an accurate determination of elastic properties and stress-strain curve requires displacement resolution of the order $\Delta U \approx 4 \times 10^{-4}$ mm. The required displacement resolution was obtained by adaptation of the technique for the precision compression test. This method was described in detail elsewhere, KLEPACZKO [13, 14]. Shortly, a disc specimen to be tested is inserted between the upper and lower platens of a testing machine, and the relative displacement δ between the platens is moni-

tored by two displacement transducers (LVDT). After securing the electric signals from both the load cell and two LVDT's it is possible to obtain a record of force P vs. displacement δ. An alternate configuration, applicable for short-time loading, consists of a digital oscilloscope to record both $P(t)$ and $\delta(t)$ as a function of time.

Due to high resolution of the measuring system and the small displacement δ_f at the crushing point, the compliance of the loading system must be taken into consideration. The compliance is usually determined by using a dummy specimen of the same geometry as specimen to be tested, made of hard aluminium alloy with known elastic properties. Force-displacement record with the dummy specimen $P(\delta)_c$ constitutes the calibration of the loading system. The net displacement of the specimen faces is equal

$$\Delta l = \delta(P) - \delta_c(P), \tag{2.1}$$

where $\delta_c(P)$ is the compliance. The compression strain can be calculated from the formula

$$\varepsilon(P) = \frac{1}{l_0}[\delta(P) - \delta_c(P)]. \tag{2.2}$$

The compliance once determined remains essentially constant for the same specimen geometry and the loading setup. Since the procedure of $\sigma(\varepsilon)$ calculation is usually performed using computer, the analytic form of the compliance can be assumed with a good approximation as

$$\delta_c = A_0 P + A_1 P^{\alpha} \tag{2.3}$$

with three constants A_0, A_1 and $\alpha, \alpha \geq 1$.

The technique of the precission compression test enables one to determine the characteristic points, besides Young's modulus, as shown schematically in Fig. 1. A complete $\sigma(\varepsilon)$ curve for a rock or a rock-like material consists basically of three regions: the elastic response, up to $(\sigma_{f_0}, \varepsilon_{f_0})$, the nonlinear part, up to $(\sigma_f, \varepsilon_f)$, i.e. the crushing point defined as P_{max} or $dP/d\delta = 0$, and the post-critical part associated with catastrophic disintegration of specimen. If strain rate $\dot{\varepsilon}$ is changed, the higher strain rate produces the curve number 2 with a positive rate sensitivity. In some rock-like materials like coal an increase of Young's modulus is frequently observed at higher strain rates, [13, 14].

The present analysis of experimental data will be limited to the point $(\sigma_f, \varepsilon_f)$ as a function of strain rate.

In order to cover the widest possible rate spectrum the compression tests were performed using three different experimental setups. The lowest and medium-low strain rate region was covered by the standard screw-driven testing machine 200 kN with computer control ($3.12 \times 10^{-5}\,s^{-1} < \dot{\varepsilon} < 1.04 \times 10^{-2}\,s^{-1}$). The test data were stored in the diskettes and later analysed.

The medium strain rates ($3.2\,s^{-1} < \dot{\varepsilon} < 7.3\,s^{-1}$), a narrow range, have been covered with the closed-loop, fast hydraulic testing machine 100 kN. The electric signals from the load cell and displacement gauges were recorded by 4-channel digital storage oscilloscope. Next the data were stored in the diskettes and the hard copy of each record was produced. Elimination of time allowed for construction of $P(\delta)$ and $\sigma(\varepsilon)$ plots.

Finally, the highest strain rates were achieved by application of the Split Hopkinson Pressure Bar (SHPB). This part of experimental program will be discussed later, ($\dot{\varepsilon} = 5 \times 10^2\,s^{-1}$).

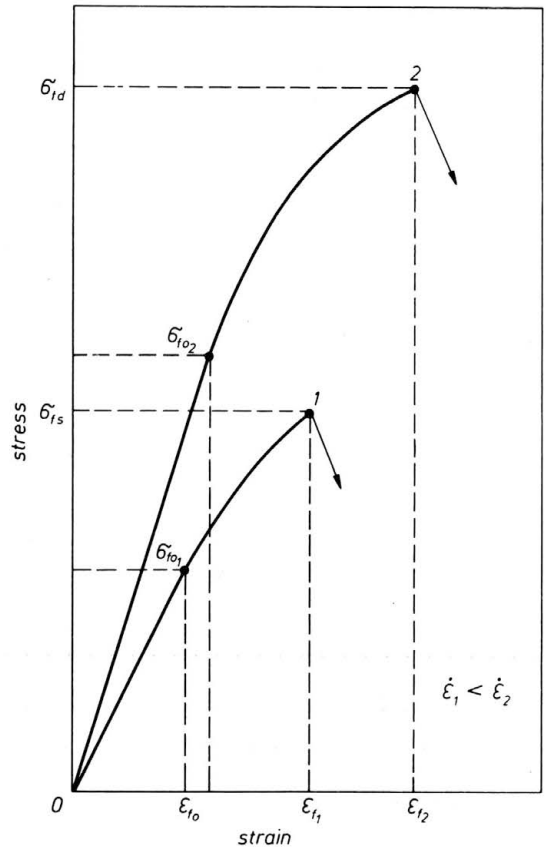

FIG. 1. Schematic stress vs. strain curves for rock and rock-like materials at two strain rates, $\dot{\varepsilon}_2 > \dot{\varepsilon}_1$; $(\sigma_{f_0}, \varepsilon_{f_0})$ the point where the curvature is detectable, $(\sigma_f, \varepsilon_f)$ the point of crushing.

In all cases of testing the same platen material was applied, i.e. a hard 2024 Al alloy, from which the Hopkinson bars were made. Specimen faces were lubricated by grease with MoS_2 base.

Within the range of the lowest and medium-low strain rates the following values of strain rates were employed: $3.12 \times 10^{-5}\,s^{-1}$; $1.04 \times 10^{-4}\,s^{-1}$; $1.04 \times 10^{-3}\,s^{-1}$; $1.04 \times 10^{-2}\,s^{-1}$; $1.2 \times 10^{-2}\,s^{-1}$. The mean value of strain rate obtained with the closed-loop hydraulic machine $\dot{\varepsilon} = 5.25\,s^{-1}$ was specially chosen as the mean between $10^{-2}\,s^{-1}$ and $5 \times 10^{2}\,s^{-1}$. For each strain rate five good tests have been completed.

Three representative curves: true stress vs. apparent strain (without elimination of stiffness) for three strain rates are shown in Fig. 2. Their significance lies in the fact, as it is discussed in the further section of this paper, that higher strain rate produces substantial reduction of the crushing strain ε_f. Also, the crushing stress σ_f has been substantially reduced when strain rate was increased. For small strains, $\varepsilon_{f_0} \leq \varepsilon \leq \varepsilon_f$, a positive rate sensitivity of stress is observed. Those results differ from the typical responses for rocks at different strain rates and such behavior of MDPA salt will be discussed further on.

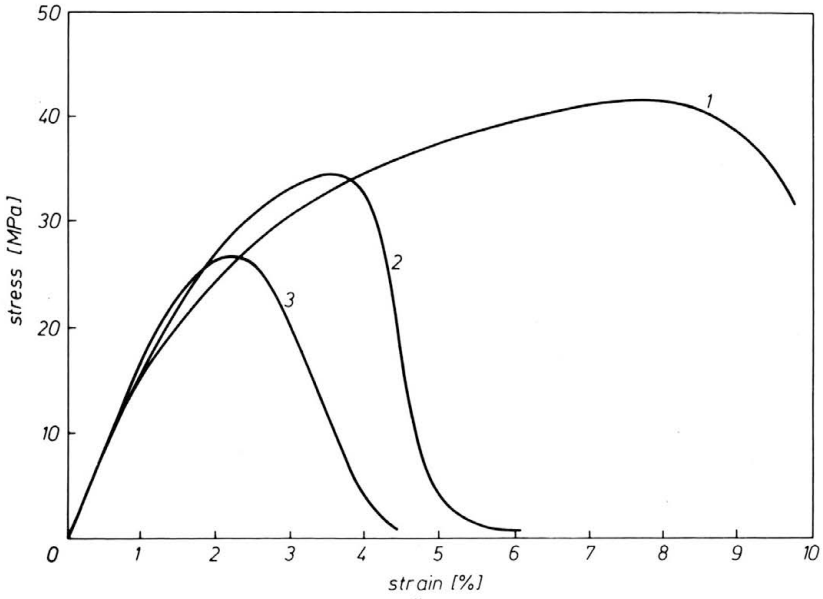

FIG. 2. Three representative curves for MDPA salt for three strain rates: $1 - \dot{\varepsilon} = 3.12 \times 10^{-5}\,s^{-1}$; $2 - \dot{\varepsilon} = 1.04 \times 10^{-2}\,s^{-1}$; $3 - \dot{\varepsilon} = 5.32\,s^{-1}$.

3. Dynamic compression tests

The high strain rate tests were performed with the SHPB apparatus specially constructed at École Polytechnique (Paris) for testing rocks and rock-like materials. All designing is similar to that implemented in the University of Manitoba, Canada, KLEPACZKO [13]. The modern SHPB apparatus consists of an air gun, Hopkinson bars and a shock absorber. The SHPB technique was developed initially for testing metals at high strain rates ($\sim 10^3 s^{-1}$), KOLSKY [15], and later found application in the testing of many materials, including rocks with or without confining the pressure, for example LINDHOLM *et al.* [4]. The most popular version, with application of mechanical impact instead of explosives, is due to LINDHOLM [16]. This version, where a short cylindrical specimen, in the present case of the same geometry as that for the quasi-static tests, is inserted between two slender bars of diameter $D = 38$ mm, is called the three-bar arrangement. The third bar is simply a projectile of the same material and diameter as the Hopkinson bars.

The loading stress pulse is initiated by the impact of the striker (third bar) against the incident bar. The striker bar is accelerated to the impact velocity v_0 by the gas gun. The amplitude ε_I of the incident pulse is proportional to the impact velocity v_0. The duration of the incident pulse is proportional to the length of the striker. Upon impact, an incident compression pulse of amplitude ε_I is propagated at the elastic wave speed $C_0 \approx 5$ mm/μs. The incident pulse propagating along the incident bar reaches the specimen and is partly reflected as a tension pulse $-\varepsilon_R(t)$ and is partly transmitted through the specimen into the transmitter bar as a compression pulse $\varepsilon_T(t)$. The relative magnitudes of the reflected ε_R and transmitted ε_T pulses depend upon the mechanical response of the specimen. Since numerous internal wave reflections occur in the specimen during the loading time

$0 \leq t \leq t_f$, where t_f is the instant of crushing (or time reading at the maximum force), the specimen remains near the mechanical equilibrium. This is the fundamental assumption of the SHPB method. The condition of mechanical equilibrium is approximately satisfied when the number of internal wave reflections is larger than 7 to 10.

If the continuous elastic strain-time histories of the incident $\varepsilon_I(t)$, reflected $-\varepsilon_R(t)$, and transmitted $\varepsilon_T(t)$ waves are recorded, then it is possible to determine the complete deformation history of a specimen material, i.e. $\sigma(\varepsilon), \dot{\varepsilon}(\varepsilon)$ and other characteristics. In the case of semi-brittle materials, including rock salt, it is difficult to satisfy the condition of mechanical equilibrium, and frequently a more exact analysis of the $\varepsilon_I(t) - \varepsilon_R(t)$ and $\varepsilon_T(t)$ records must be employed.

Technical details of the SHPB apparatus used in the rock salt testing will be omitted here. It may be important to describe some basic data of the SHPB. Impact velocity v_0 was measured by three photodiodes and digital memories. The system of three photodiodes allows for determination of the assumed constant acceleration or deceleration of the projectile just before impact, and then an exact value of v_0 can be determined. The waves $\varepsilon_I, \varepsilon_R$ and ε_T were measured by SR gauges with the gauge length 3 mm. The signals after conditioning were stored in the memory of the digital oscilloscope and next the digital data were stored on a disk for further computer analyses.

Due to the tendency found from the quasi-static tests that the crushing strain ε_f substantially diminishes at increasing strain rates, the problem of mechanical equilibrium and other effects associated with the interface friction, radial and longitudinal inertia of specimen, Pochhamer–Chree vibrations (radial inertia of Hopkinson bars of diameter 38 mm) become more important in the analysis of oscillograms.

In order to improve oscillogram analysis and to determine the stress-strain characteristics more exactly, the computer program DAVID has been specially prepared for this purpose, GARY and KLEPACZKO [17]. If the three waves $\varepsilon_I, \varepsilon_R$ and ε_T are stored in the digital form and the impact velocity v_0 of the projectile is known, the data can be fully analysed using the program DAVID. The effects of inertia and friction are included into the program using the analytic formula derived in [11]. The following formula for the elimination of the effects of friction and inertia has been implemented into the program DAVID

$$\sigma(t) = \overline{\sigma}_z(t)\left(1 - \frac{\mu}{3s(t)}\right) + \rho\frac{d^2(t)}{12}\left[s^2(t) - \frac{3}{16}\right][\dot{\varepsilon}^2(t) + \ddot{\varepsilon}(t)] + \frac{3\varrho d^2(t)}{64}\ddot{\varepsilon}(t), \tag{3.1}$$

where $\sigma_z(t)$ is the calculated value of the mean true compression stress as a function of time with the standard SHPB analysis of waves, KLEPACZKO [18,19]; $s(t) = 1/d$ is the current value of the aspect ratio, $\dot{\varepsilon}(t)$ and $\ddot{\varepsilon}$ are, respectively, the current mean values of strain rate and acceleration as calculated from SHPB formulas, μ is the coefficient of friction, finally σ is the current value of the corrected stress. It is important to note that during SHPB test the mean strain rate $\dot{\varepsilon}$ and the mean strain acceleration $\ddot{\varepsilon}$ are not constant and they must be determined during the data analysis with the SHPB procedures.

In addition to the standard SHPB procedures, the program DAVID allows for the complete analysis of the energy absorption in the specimen volume. The energy formulas have been discussed by KLEPACZKO [18]. A more simple analysis of this kind was reported by LUNDBERG [20]. The energy analysis enabled computer calculations of the energy of crushing W_m as a function of the mean strain rate $\dot{\varepsilon}$.

Generally, the program DAVID enables one to calculate 30 different functions, includ-

ing the corrected mean stress, the forces and displacements at both faces of the specimen. Such procedure can be used for evaluation of the test as well as for the complete determination of stress or strain errors due to temporary loss of mechanical equilibrium. Among others, the following functions can be calculated and displayed: $\sigma(t)$, $\varepsilon(t)$, $\sigma(\varepsilon)$, $\dot{\varepsilon}(\varepsilon)$, $W_m(\varepsilon)$, etc.

4. Experimental results for the whole rate spectrum

Having completed experiments with three setups which cover the wide rate spectrum, it was possible to construct the following three plots:

i. crushing stress σ_f vs. logarithm of strain rate, $\log \dot{\varepsilon}$, shown in Fig. 3;
ii. crushing strain ε_f vs. logarithm of strain rate, $\log \dot{\varepsilon}$, shown in Fig. 4;
iii. crushing energy W_m vs. logarithm of strain rate, $\log \dot{\varepsilon}$, shown in Fig. 5.

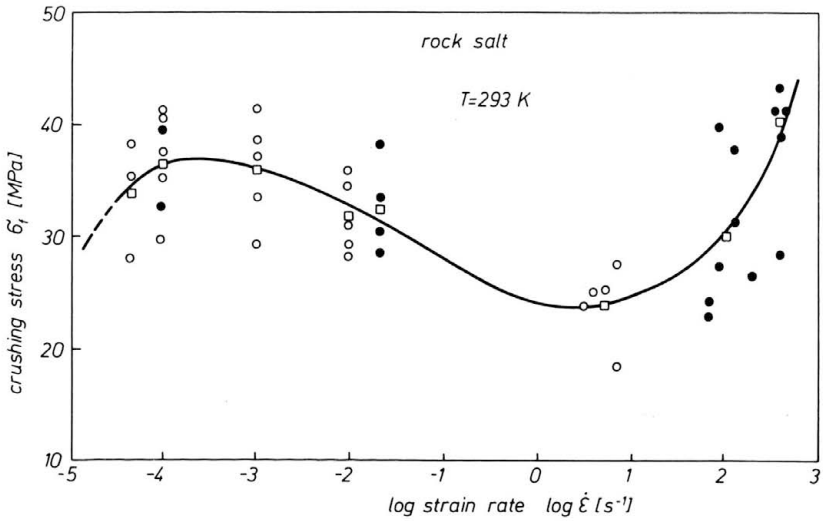

FIG. 3. Rate spectrum of crushing stress σ_f for MDPA rock salt; ○ — experimental data of Metz University, • — experimental data of École Polytechnique, □ — mean values.

Figure 3 reveals rather complicated and non-typical changes of the crushing stress as a function of $\log \dot{\varepsilon}$.

The strain rate sensitivity of halite and natural rock salts has been determined many times from creep tests, for example in a review paper by CARTER and HANSEN [21]. If the following definition of rate sensitivity of uniaxial stress ($p = 1/3\sigma$) is introduced, where p is the hydrostatic component of the stress tensor, $p = 1/3\sigma_{kk}$

$$\beta = \left(\frac{\partial \sigma}{\partial \log \dot{\varepsilon}}\right)_{T,p}, \tag{4.1}$$

then up to the strain rate $\dot{\varepsilon} \approx 10^{-4}\,\mathrm{s}^{-1}$ the rate sensitivity of crushing stress β_f is positive. Consequently Eq. (4.2) defines β_f

$$\beta_f = \left(\frac{\partial \sigma_f}{\partial \log \dot{\varepsilon}}\right)_{T,p}. \tag{4.2}$$

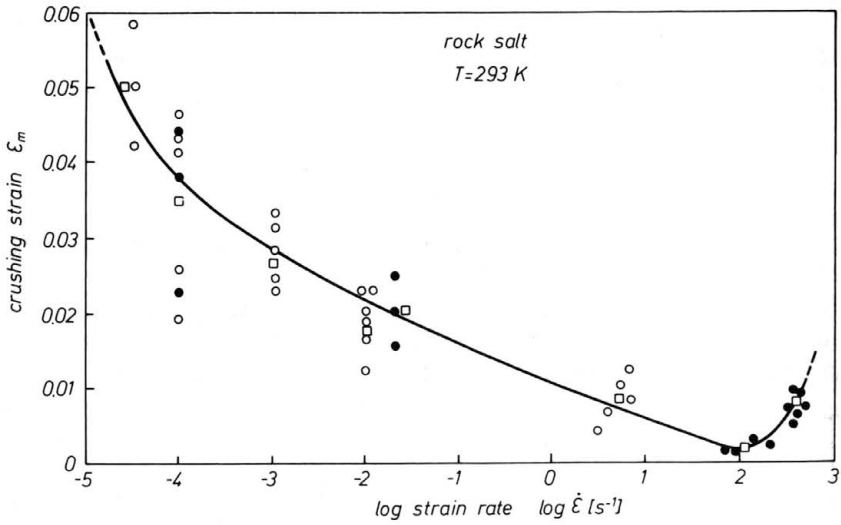

FIG. 4. Rate spectrum of crushing strain ε_f for MDPA rock salt; ○ — experimental data of Metz University, ● — experimental data of École Polytechnique, □ — mean values.

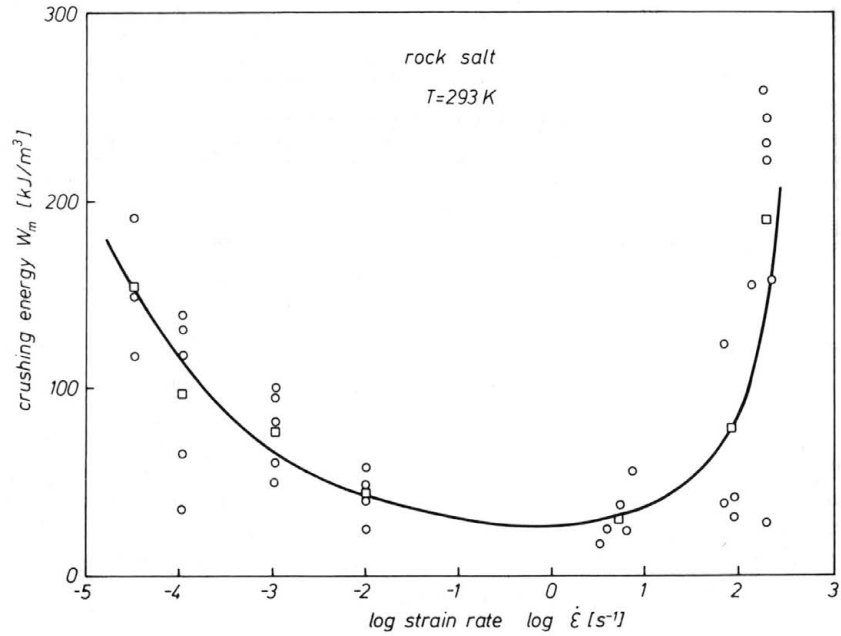

FIG. 5. Rate spectrum of crushing energy W_m for MDPA rock salt; ○ — experimental data, □ — mean values.

For example, the order of β determined from the experimental data for rock salt reported by FARMER and GILBERT [22], where constant strain rate tests were performed within the range $2\times10^{-7}\,s^{-1} < \dot{\varepsilon} < 5\times10^{-3}\,s^{-1}$, is $\beta = 5.5$ MPa for deformation $\varepsilon = 0.04$.

Similar positive values of β were determined for $\varepsilon = 0.02$ and $\varepsilon = 0.10$ using data of Fig. 14 published by FARMER and GILBERT [22]. The slope $\Delta\sigma_f/\Delta\log\dot{\varepsilon}$ of Fig. 3 fits the value of $\beta = 6$ MPa at strain rates lower than $1 \times 10^{-4}\,s^{-1}$. This is the creep region in Fig. 3. The next part of the plot $\sigma_f(\log\dot{\varepsilon})$, between the strain rates $1 \times 10^{-4}\,s^{-1} < \dot{\varepsilon} <\sim 1\,s^{-1}$, is characterized by the *negative* rate sensitivity β_f of crushing stress. The lowest rate sensitivity of β_f occurs at $\dot{\varepsilon} \approx 3 \times 10^{-2}\,s^{-1}$ and its value is $(\beta_f)_{\min} = -4.48$ MPa. It is believed that the negative values of β_f within this strain rate region are due to enhanced microcracking superimposed on plastic deformation. Such point of view that the effect of increased strain rate is to make the rock salt specimens appear more brittle was deduced from the state of the tested specimens by FARMER and GILBERT [22].

The minimum of σ_f is observed approximately at strain rate $\dot{\varepsilon} = 2.0\,s^{-1}$. Finally, within the region of high strain rates $50\,s^{-1} < \dot{\varepsilon} < 10^3\,s^{-1}$, σ_f rises again. The positive effect of high strain rates on σ_f is due to microcracking inertia superimposed on the increased hydrostatic component p of the stress tensor developed by the radial inertia of the specimen material, KIPP *et al.* [23], KLEPACZKO [24], JANACH [25].

The role of microcracking, microcracking inertia and an increase of the hydrostatic component of the stress tensor at high strain rates will be discussed further in the next part of this paper.

Even more dramatic changes of the crushing strain ε_f as a function of $\log\dot{\varepsilon}$, in comparison to σ_f, are shown in Fig. 4. Those results demonstrate a substancial reduction of plasticity and enhanced damage due to microcracking when strain rate is increased. The increase of $\dot{\varepsilon}$ from $1 \times 10^{-4}\,s^{-1}$ to $10^2\,s^{-1}$, i.e. six decimal orders, reduces the crushing strain from $\sim 4 \times 10^{-2}$ to $\sim 2 \times 10^{-3}$. Specimens tested with the SHPB at $\dot{\varepsilon} \approx 10^2\,s^{-1}$ showed almost brittle fracture with small values of ε_f (of the order $\sim 2 \times 10^{-3}$). An increase of the hydrostatic component of the stress tensor and microcracking inertia at the highest strain rate $\dot{\varepsilon} \approx 5 \times 10^2\,s^{-1}$ produced increase of ε_f up to $\sim 1 \times 10^{-2}$.

Because at the medium strain rates an increase of strain rate reduces both σ_f and ε_f, it was obvious that the crushing energy will also show substantial changes as a function of strain rate. The integration procedures and the program DAVID have been used to calculate $W_m(\log\dot{\varepsilon})$, and the results are shown in Fig. 5. Again, a deep minimum of W_m is clearly visible at $\dot{\varepsilon} \approx 1.0\,s^{-1}$. At the highest strain rates the scatter of both quantities σ_f and ε_f enhanced the scatter of W_m. However, the two mean values of W_m show a substantial increase.

Since the reported results obtained within a wide spectrum of strain rates for the MDPA rock salt demonstrate new features, not reported in the open literature so far, a more complete discussion is attempted in the next part of this paper.

5. Discussion of experimental results, quasi-static and medium rates

It is obvious that the observed changes of σ_f, ε_f and W_m stem from the physical phenomena present at different strain rates. Diffusion, plasticity (motion of dislocations), microcracking, inertia of microcracking and effects of hydrostatic pressure are usually superimposed in different proportions depending on conditions of loading, i.e. temperature, strain rate, stress (creep), strain (stress relaxation) and confining pressure. Those factors will influence not only the flow stress and rate sensitivity but also the mode of failure. Analysis of the available experimental data for rocks and rock-like materials reveals two typical schemes as shown in Fig. 6a and 6b, after MRÓZ and ANGELILLO [26]. When

plasticity dominates during specimen deformation at increased strain rates, the result of uniaxial compression tests will be as shown in Fig. 6a, where $\dot{\varepsilon}_1 < \dot{\varepsilon}_2 < \dot{\varepsilon}_3$. The increase of both the crushing stress σ_f and crushing strain ε_f is observed, the loci of points $(\sigma_f, \varepsilon_f)$ constitute the failure envelope. The rate sensitivity of stress β and the rate sensitivity of crushing stress β_f are both positive. The arrow shows direction of changes of the envelope when strain rate is increased.

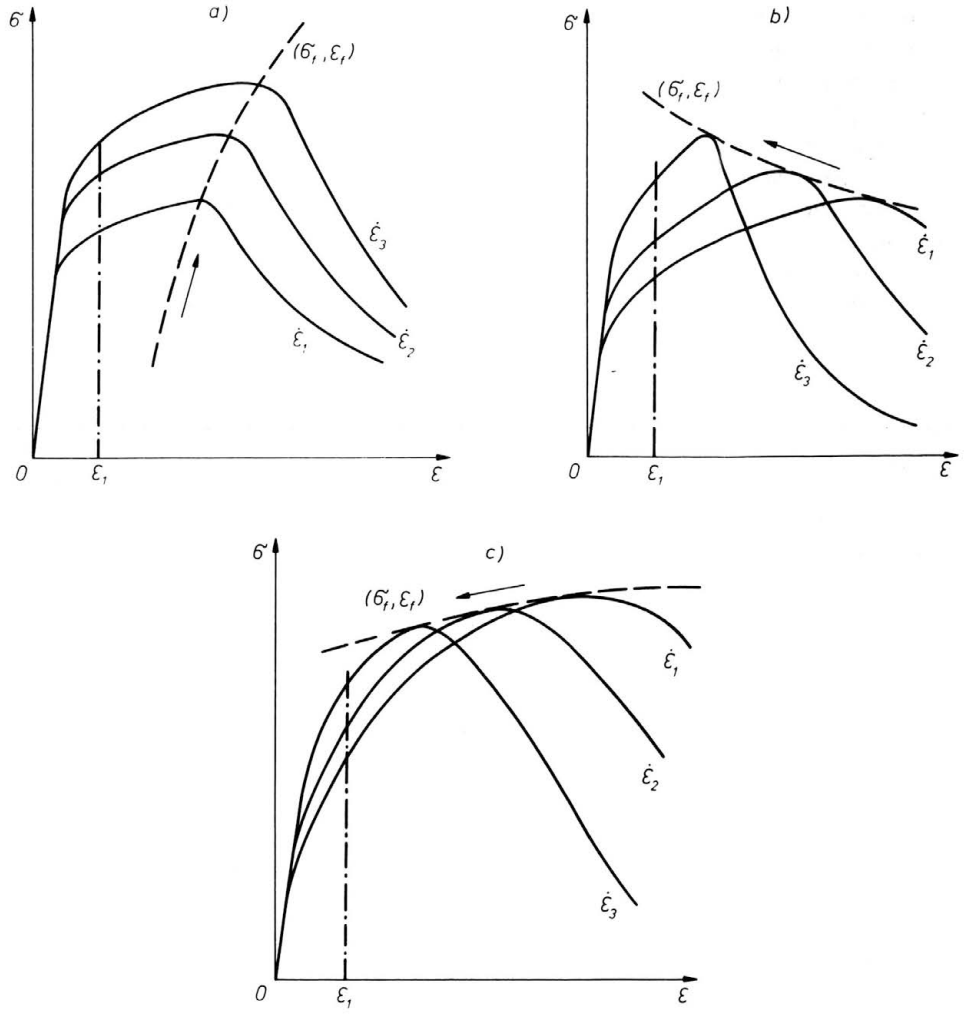

FIG. 6. Three possibilities of specimen behaviour loaded at different rates in uniaxal compression for rock or rock-like materials; (σ_f, ε) denotes the failure loci (dashed lines); $\dot{\varepsilon}_1 < \dot{\varepsilon}_2 < \dot{\varepsilon}_3$.

For the second case, shown in Fig. 6b, the crushing stress σ_f increases when the strain rate is increased, but at the same time the crushing strain ε_f decreases at increased strain rates. Such behavior indicates an embrittlement of material due to increased strain rate. Both strain rate sensitivities β and β_f are positive.

Finally, the case shown in Fig. 6c depicts the behavior of the MDPA rock salt in the domain of small and medium strain rates. For this case an enhanced embrittlement reduces not only ε_f but also σ_f leading to a deep minimum of the crushing energy W_m. Moreover, the rate sensitivity β_f of crushing stress is *negative*.

It is important to note, looking at all schematic figures a, b and c, that in the case of small strains of the order $\sim \varepsilon_1$ the rate sensitivity β of the current stress is always positive.

6. Remarks on constitutive modeling

The next part of this paper will be briefly focussed on constitutive modeling of the phenomena which have lead to the material response shown in Fig. 6c.

Although natural aggregates of the rock salt contain appreciable concentration of impurities in the form of silt and clay layers, the dominant bulk material is halite. Thus, it is reasonable to study the constitutive laws formulated for single crystals or polycrystals of pure halite.

At moderately low temperatures, $\theta \approx 0.4$, where θ is homologous temperature, ($\theta = T/T_m$, T_m is the melting temperature in [K]) and strain rates higher than $\sim 10^{-5}\,\mathrm{s}^{-1}$, the plastic deformation in halite occurs by dislocation glide. If motion of dislocation is thermally activated, then the general Arrhenius relation defines the shear strain rate $\dot{\Gamma}$, for example KLEPACZKO [27].

$$\dot{\Gamma} = \nu_i(s_j) \exp\left[-\frac{\Delta G_i(\tau^*, s_j)}{kT}\right], \tag{6.1}$$

where ν_i is the frequency factor and ΔG_i is the free energy of activation, k is Boltzmann constant and T the absolute temperature. The subscript i indicates the i-th, so far unspecified, thermally activated micro-mechanism of plastic deformation. Since plastic deformation is associated with generation and annihilation of defects (dislocations), both the frequency factor ν_i and free energy ΔG_i must depend on microstructure characterized by s_j structural variables, KLEPACZKO, [29]. Generally, ΔG depends on the effective shear stress τ^* in a nonlinear manner, where $\tau^* = \tau - \tau_\mu$, τ is the applied stress and τ_μ is the internal stress, for example KOCKS *et at.* [28]. The free energy of activation ΔG can be written in the linear case as follows:

$$\Delta G_i = \Delta H_i - v^* \tau^*, \tag{6.2}$$

where ΔG is the activation energy for the particular case of dislocation glide. The coefficient v^*, having the dimension of volume, is called the activation volume; also from Eq. (6.2) $v^* = -dG/d\tau^*$. The activation volume v^* is a critical parameter in the thermal activation strain rate analysis. The rate sensitivity β_τ is directly related to the activation volume v^*

$$v^* = \left(\frac{kT}{\beta_\tau}\right)_{T,p}, \quad \text{or } v^* = \left(\frac{kT}{m\tau}\right)_{T,p}, \tag{6.3}$$

where β_τ and m_τ are the rate sensitivities, [27]

$$\beta_\tau = \left(\frac{\partial \tau}{\partial \log \dot{\Gamma}}\right)_{T,p} \quad \text{and} \quad m = \left(\frac{\partial \log \tau}{\partial \log \dot{\Gamma}}\right)_{T,p}. \tag{6.4}$$

When Tresca yield condition is assumed, i.e. $\sigma = 2\tau$, the activation volume v^* can be calculated at room temperature using the value of $\beta_\sigma = 5.5$ MPa and the value of kT at

$T = 300$ K, $kT = 4.134 \times 10^{-21}$ J, $v^* = 1.51 \times 10^{-27}$ m^3. The ratio to Burgers displacement $b = 4 \times 10^{-10}$ m gives finally the following value $v^*/b^3 = 23.5$. This relatively small value of v^* suggests that the intrinsic lattice resistance to dislocation glide participates in plastic deformation of halite at RT. It must be, however, remembered that the value $v^*/b^3 = 23.5$ has been determined for the natural rock salt. ARIELI *et al.*, [30] determined the activation volumes for annealed polycrystalline pure halite at temperatures $296\text{K} \leq T \leq 673\text{K}$ and strain rates $10^{-8}\text{s}^{-1} \leq \dot{\varepsilon} \leq 10^{-1}\text{s}^{-1}$. The values of v^*/b^3 found within the temperature range $296\text{K} \leq T \leq 423\text{K}$ were strain-independent and they changed from $v^*/b^* \approx 3.5$ at $T = 296\text{K}$ to $v^*/b^3 = 6.0$ at $T = 423\text{K}$.

A more general analysis of available dislocation mechanisms which control plastic deformation of halite at different temperatures is possible via deformation mechanism maps, FROST and ASHBY [31], MUNSONand DAWSON, [32]; BLUM and FLEISCHMANN [33]. Two dislocation mechanisms which can contribute to plastic flow, in addition to the Peierls one, are dislocation climb and dislocation cross-slip. It is expected that the climb will dominate at medium-high homologous temperatures and the cross-slip will prevail at high stresses and relatively low homologous temperatures, SKROTZKI and HAASEN, [34]. Unfortunately, both mechanisms lead to the similar constitutive relation

$$\dot{\Gamma} = \dot{\Gamma}_{0i}\left(\frac{\tau^*}{\mu}\right)^{1/m} \exp\left[-\frac{\Delta H_i(T)}{kT}\right], \tag{6.5}$$

where ΔH_i is the stress-independent activation energy for i-th mechanism (climb or cross-slip), μ is the elastic shear modulus, τ^* is the effective stress and $\dot{\Gamma}_{0i}$ is a constant. The logarithmic rate sensitivity m is defined at constant T and p by Eq. (6.5). When Eq. (6.5) is inverted and Tresca yield condition is assumed, i.e. $\tau^* = \sigma^*/2$, $\dot{\Gamma} = 2\dot{\varepsilon}$, one can determine the flow stress

$$\sigma = \sigma_\mu + 2\mu\left(\frac{2\dot{\varepsilon}}{\dot{\Gamma}_{0i}} \exp\left(\frac{\Delta H_i(T)}{kT}\right)\right)^m. \tag{6.6}$$

Introduction of the Zener-Hollomon parameter Z, where

$$Z = \dot{\varepsilon} \exp\left(\frac{\Delta H_i}{kT}\right) \tag{6.7}$$

yields

$$\sigma = \sigma_\mu + 2\mu\left(\frac{Z}{\dot{\varepsilon}_{0i}}\right)^m, \quad \dot{\varepsilon}_{0i} = \dot{\Gamma}_{0i}/2. \tag{6.8}$$

Since the logarithmic rate sensitivity m is related to the rate sensitivity of stress β_σ by the following relation, KLEPACZKO [27], $m_f = \beta_\sigma/\sigma_f$, value of m_f can be found for the MDPA rock salt using value $\beta_\sigma = 5.5$ MPa and $\sigma_f = 34.2$ MPa at $\dot{\varepsilon} = 3 \times 10^{-5}\text{s}^{-1}$; the value is $m_f = 0.161$ or $m_f^{-1} = 6.22$. This value correlates well with the values given in literature, for example NEVILLE *et al.* [34], $m^{-1} = 7$.

Equation (6.6) is an ample source of phenomenological constitutive modeling. It is usually assumed that $\sigma_\mu = 0$ and $\Delta H = \text{const}$, then

$$\sigma = B\dot{\varepsilon}^m, \quad B = 2\mu\left(\frac{2}{\dot{\Gamma}_{0i}}\right)^m \exp\left(\frac{m\Delta H}{kT}\right). \tag{6.9}$$

Of course, strain hardening is eliminated due to assumption of the steady state (no evolution of microstructure).

Fundamental assumption in phenomenology of constitutive modeling for rock salt is the concept of mechanical equation of state

$$(\sigma, \varepsilon, \dot{\varepsilon}, T) = 0, \tag{6.10}$$

where all four quantities constitute the four-dimensional surface and stress σ follows any path on the surface. There is no evolution of microstructure in the model and strain acts as an independent variable. Strain rate and temperature may be related by physical relations. The specific case of the constitutive surface is in the form

$$\sigma = f_1(\varepsilon) f_2(\dot{\varepsilon}) f_3(T), \quad p = \text{const}. \tag{6.11}$$

This uncoupled form is used frequently for many materials. A more specific form is as follows:

$$\sigma = f_1(\varepsilon)\dot{\varepsilon}^m \exp\left(\frac{Q}{T}\right), \quad p = \text{const}, \tag{6.12}$$

where $f_1(\varepsilon)$ represents the effect of strain hardening, m is defined above and Q is a constant. Relation (6.12) can be rewritten with the Zener—Hollomon parameter

$$\sigma = f(\varepsilon) Z^m, \quad p = \text{const}. \tag{6.13}$$

The empirical power law for transient creep of the form

$$\varepsilon_c = A t^s \sigma^r T^q, \tag{6.14}$$

applied for two rock salts by NEVILLE *et al.* [21] with $s_1 = 0.45$; $r_1 = 3.3$ and $q = 11.4$ and $s_2 = 0.3$ and $q_2 = 9.5$, can be rearranged into

$$\sigma = B\varepsilon^n \dot{\varepsilon}^m T^{-1}, \tag{6.15}$$

where $n = (1 - s)/r$; $m = s/r$; $l = q/r$ and $n_1 = 0.167$; $m_1 = 0.136$; $l_1 = 3.45$, for the second case: $n_1 = 0.233$; $m_2 = 0.100$; $l_2 = 3.17$.

Another form of the mechanical equation of state of the power form has been applied for the rock salt by RUSSEL *et al.* [35]. The form of Eq. (6.12) was applied with $f_1(\varepsilon) = B\varepsilon^n$. It has been concluded that the strain hardening index n remains constant only at medium strains and the steady-state cannot be predicted. Those authors finally introduced, as $f_1(\varepsilon)$ in Eq. (6.11), a combination of exponential functions. The total number of constants in that equation of state was five.

It can be shown that for many materials the most general form of the mechanical equation of state in the power form obeys the relation, KLEPACZKO [36, 37],

$$\sigma = B(T)\varepsilon^{n(T)}\dot{\varepsilon}^{m(T)}, \quad p = \text{const}, \tag{6.16}$$

where $B(T)$, $n(T)$ and $m(T)$ are, respectively, the plasticity modulus, strain hardening index, logarithmic rate sensitivity. The final form of the constitutive relation (6.16) has been analysed in [36] and the result is the set of Eqs. (6.17) to (6.21)

$$\tau = \hat{\tau}\left[\frac{\dot{\Gamma}}{\dot{\Gamma}_0}\exp\left(\frac{\Delta H}{kT_m\theta}\right)\right]^{m(\theta)}, \tag{6.17}$$

$$\hat{\tau} = C(\theta)(\Gamma_0 + \Gamma)^{n(\theta)}, \tag{6.18}$$

$$C(\theta) = [1 - (\theta - p)\exp(q(1 - \theta))], \tag{6.19}$$

$$m(\theta) = \alpha_m \theta, \quad 0 < \theta \leq 0.5, \tag{6.20}$$

$$n(\theta) = n_0(1-\theta), \quad 0 < \theta < 1, \tag{6.21}$$

where $\theta = T/T_m$ and T_m is the melting temperature, k is Boltzmann constant; ΔH, Γ_0, $\dot{\Gamma}_0$, p, q, α_m and n_0 are material constants. This constitutive set can be applied to the modeling of strain rate and temperature effects in pure polycrystalline halite within wide range of homologous temperatures, $0 < \theta \leq 0.5$. In addition, it is recommended to use the *inelastic* strain ε_i; in all equations of the power form, $\varepsilon_i = \sigma/E - \varepsilon$.

All constitutive relation discussed above are related to the time-dependent plasticity and they are not capable of taking into account the effect of microcracking on σ and σ_f. It is possible to introduce in Eq. (6.1) the function of damage

$$\sigma = f_1(\varepsilon, T) f_2(\dot{\varepsilon}, T) f_3(T) f_4(D, \dot{\varepsilon}). \tag{6.22}$$

The first two schematic diagrams of Fig. 6 indicate the negative rate-dependence of the crushing stress. MRÓZ and ANGELILLO [26] assumed a damage rule due to deformation degradation and stress degradation. However, in the present case a different approach will be pursued. It has been assumed that the probability of damage D can represent strain and rate-dependent material deterioration, $0 \leq D \leq 1$, and a less general form of $f_4(D)$ is

$$f_4(D, \varepsilon) = 1 - D(\varepsilon, \dot{\varepsilon}), \quad p = 0. \tag{6.23}$$

Since it has been found that the MDPA salt deteriorates in proportion to $\log \dot{\varepsilon}$, as it is shown in Fig. 3, the following explicit formula for $D(\varepsilon, \dot{\varepsilon})$ is proposed

$$D(\varepsilon, \dot{\varepsilon}) = \langle D_1 \rangle \left(\frac{\varepsilon}{\varepsilon_0} - 1 \right)_s + D_2 \log \left(\frac{\dot{\varepsilon}}{\dot{\varepsilon}_0} \right), \quad \begin{cases} \dot{\varepsilon} \geq \dot{\varepsilon}_0, \\ \varepsilon \geq \varepsilon_0, \end{cases} \tag{6.24}$$

where D_1, D_2, ε_0 and $\dot{\varepsilon}_0$ are material constants. The physical meaning of Eq. (6.24) stems from the experimental observation that the rate-dependent deterioration begins at the strain rate $\dot{\varepsilon}_0$ and, at the same time, the strain-dependent deterioration is triggered at ε_0. Because the strain-dependent damage starts at ε_0, the operator $\langle\,\rangle$ has been introduced: $\langle \cdot \rangle = 0$ for $\varepsilon \leq \varepsilon_0$ and $\langle \cdot \rangle = D_1$ for $\varepsilon > \varepsilon_0$. The quasi-static limit of $(\varepsilon_c - \varepsilon_0)_s$ can be, for example, determined from Fig. 2 for strain rate $\dot{\varepsilon} = 3 \times 10^{-5}\,\mathrm{s}^{-1}$; $(\varepsilon_c - \varepsilon_0) \approx 0.12$, where ε_c is maximum strain where $D = 1$. Since the minimum of ε_f can be estimated from Fig. 4 as being close to the yield strain $\varepsilon_e \approx 2.5 \times 10^{-3}$, then it is assumed that $\varepsilon_0 = \varepsilon_e$ and the constant D_1 in Eq. (6.24) has the value $D_1 = 2.13 \times 10^{-2}$. Similarly, the constant D_2 can be determined from Fig. 3. When it is assumed that $\varepsilon_0 = 10^{-4}\,\mathrm{s}^{-1}$, the negative slope of $\sigma_f(\log \dot{\varepsilon})$ extrapolated to $\sigma_f = 0$ gives the value of $\varepsilon_c \approx 10^{-5}\,\mathrm{s}^{-1}$ and $D_2 = [\log(\dot{\varepsilon}_c/\dot{\varepsilon}_0)]^{-1}$; $D_2 = 0.11$. Thus, within the domain of strain rates $10^{-4}\mathrm{s}^{-1} \leq \dot{\varepsilon} \leq 10\,\mathrm{s}^{-1}$, the tenfold increase of $\dot{\varepsilon}$ increases the rate-dependent damage by $\sim 11\%$. Of course, this simple determination of constants bears some errors and is understood as preliminary. The simple phenomenological formulas (6.23) and (6.24) can take into account in the linear form the strain- and strain-rate dependent damage in Eq. (6.22). The effect of confining pressure is neglected in this approach by assuming $p = 0$. Of course, application of confining pressure will substantially increase ε_0 and will reduce the value of D_1. It is not clear, though, whether the rate-dependent damage will remain unchanged at increasing values of p. Some preliminary data for rock salt seem to indicate that the maximum of σ_f is shifted from $\dot{\varepsilon} \approx 10^{-4}\,\mathrm{s}^{-1}$ at $p = 0$ to $10^{-3}\,\mathrm{s}^{-1}$ at $p = 5MPa$, HUNSCHE [38].

7. Discussion of experimental results, high strain rates

It has been recognized for some time that rocks and ceramics show a sudden increase in the crushing stress σ_f at strain rates above $10^2\,s^{-1}$. For example, tests performed on coal for the strain rate range $10^{-4}\,s^{-1} \leq \dot{\varepsilon} \leq 2 \times 10^3\,s^{-1}$ have shown such a behavior, KLEPACZKO [13]. A similar behavior has been found in the MDPA salt, where the crushing stress starts to increase at strain rates above $10\,s^{-1}$. At the highest strain rates, achieved by means of the SHPB, the salt tested has shown the highest strength and relatively high rate sensitivity. It is known that within the high strain-rate domain, above $\sim 10\,s^{-1}$, the rate sensitivity β or β_f is not a constant for rocks and rock-like materials, but increases very fast when strain rate is increased, for example GREEN *et al.* [6.40], KLEPACZKO *et al.* [13, 14, 39].

As there is a considerable practical interest in the high strain-rate sensitivity of rock salt under impact loading, a further discussion of this effect will be pursued. Generally, two material factors contribute to the enhancement of the rate sensitivity at high strain rates. The first one, which develops the apparent strengthening, is a direct consequence of the pressure sensitivity of the failure stress. Since the intrinsic rate sensitivity of stress increases as a function of strain rate, so it develops an increase of the mean stress $\sigma_0 = \sigma_1/3$, and in turn, an increase of the mean stress increases σ_f. In addition the effect is amplified by radial inertia of the specimen material, JANACH [25]. The pure quasi-static effect of the mean pressure on the failure stress of the rock salt has recently been demonstrated by HUNSCHE, [41]. It was shown that the strength of rock salt increases non-linearly with increasing mean stress p.

The second factor is the effect of the inertia controlled growth of Mode I micro-cracks, GRADY *et al.* [23, 42], LANKFORD [43]. At the early stages of fast loading, the crack (or microcrack) response exhibits a delayed time-dependence due to material inertia near the crack tip. Thus, higher dynamic fracture stress in region of high strain rates are of consequence of microstructural inertia effects, leading to an excessive strain rate sensitivity.

It is clear that both factors contribute at the same time, however, in different proportions depending upon the conditions of loading. A more exact discussion and derivation of constitutive relations which include both effects is published elsewhere, KLEPACZKO [24]. The total increment of crushing stress σ_f determined from experiments can be split into two components

$$(\Delta\sigma_f)_{\text{TOTAL}} = (\Delta\sigma_f)_{\text{PRESSURE}} + (\Delta\sigma_f)_{\text{RATE}}. \tag{7.1}$$

The first component is a function of the first invariant of the stress tensor, i.e. the mean pressure, whereas the second shows a cube root dependence of σ_f on strain rate, if the model proposed by GRADY *et al.* is true.

In the double logarithmic coordinates $(\log\sigma_f, \log\dot{\varepsilon})$ the model with inertia of micro-cracking should provide a straight line with the logarithmic rate sensitivity $m_f = 1/3$. Such a plot has been constructed and is shown in Fig. 7. The linear regression

$$\log\sigma_f = A + m_f \log\dot{\varepsilon} \tag{7.2}$$

is represented by the straight line with $A = 1.293$ and $m_f = 0.108$ if σ_f is in MPa and $\dot{\varepsilon}$ in s^{-1}, the regression coefficient $r^2 = 0.508$. The dashed line represents the microcracking inertia model with $m = 1/3$. It is probable that the evolution of damage can supress some part of the rate sensitivity.

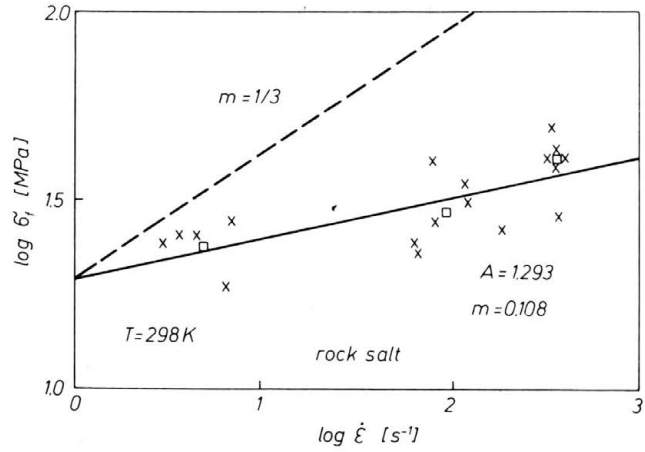

FIG. 7. Plot of $\log \sigma_f$ vs. $\log \dot{\varepsilon}$ for MDPA rock salt; × — experimental points, □ — mean values from Fig. 3, the solid line is the linear regression and the dashed line represents model with microcracking inertia, $m_f = 1/3$

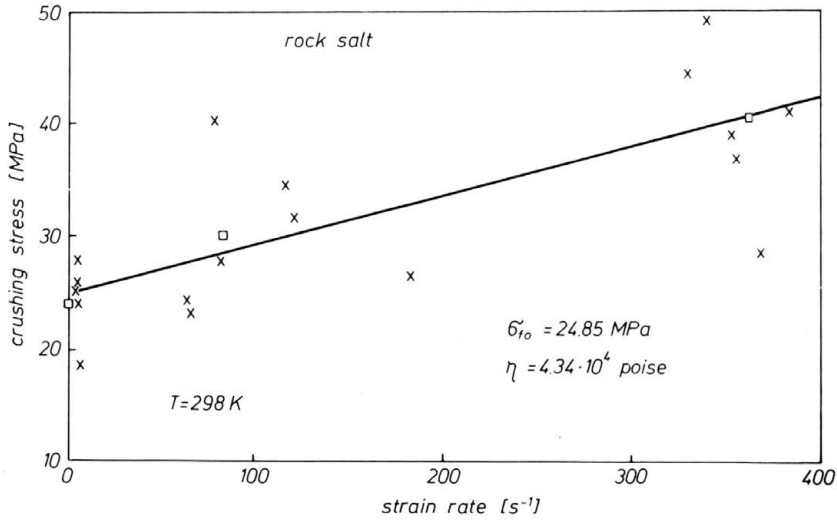

FIG. 8. Plot of σ_s vs. $\dot{\varepsilon}$ for MDPA rock salt, × — experimental points, □ — mean values from Fig. 3, the solid line is the linear regression analysis, η is pseudo-viscosity.

The second possibility to analyse the region of high strain rates is to introduce the notion of pseudo-viscosity, KLEPACZKO *et al.* [13, 14, 24, 39]. In such case the following linear relation holds

$$\sigma_f = \sigma_{f0} + \eta\dot{\varepsilon} \tag{7.3}$$

with pseudo-viscosity $\eta = (\partial\sigma_f/\partial\dot{\varepsilon})$; the dimension of η is in Pa.s, or in Poise. The linear regression analysis has been applied for experimental results on MDPA salt and the result is shown in Fig. 8. Indeed, the linear regression provides a relatively good fit to experimental points with $\sigma_{f0} = 24.85$ MPa, $\eta = 4.34 \times 10^4$ Pa.s and $r^2 = 0.57$. Thus,

the pseudo-viscosity approach gives even better r^2 than the case of Eq. (7.2). The order of pseudo-viscosity η is the same as the mean values determined for example for coal $\eta = 3.66 \times 10^4$ Pa.s and mortars $\eta = 4.27 \times 10^4$ Pa.s aged 28 days, and $\eta = 5.95 \times 10^4$ Pa.s for mortar aged 6 months, KLEPACZKO [39].

8. Conclusions

Evidence has been presented for strain-rate dependent failure of the MDPA salt in compression without confining pressure. Certainly, the experimental results show that the crushing stress σ_f, the crushing strain ε_f and the crushing energy W_m are complicated functions of the strain rate $\dot{\varepsilon}$. The maximum of the crushing stress σ_f is observed at $\dot{\varepsilon} \approx 10^{-4}\,\mathrm{s}^{-1}$. At low strain rates, $\dot{\varepsilon} \leq 10^{-4}\,\mathrm{s}^{-1}$, plasticity dominates over the damage processes. But at higher strain rates, $10^{-4}\,\mathrm{s}^{-1} \leq \dot{\varepsilon} \leq 1\,\mathrm{s}^{-1}$, the damage dominates over intrinsic rate sensitivity, and the crushing stress σ_f, the crushing strain ε_f and the crushing energy W_m exhibit negative rate sensitivity, a very important engineering problem. Finally, at high strain rates, $\dot{\varepsilon} \geq 10\,\mathrm{s}^{-1}$, the effect of mean pressure and microcracking inertia are the main factors which make the rate sensitivities of σ_f, ε_f and W_m positive. However, the logarithmic rate sensitivity m_f is lower than that predicted by the microcracking inertia model. Probably the rate sensitivity is supressed by some damage processes which accompany the inertia of microcracking. Further studies are needed to combine intrinsic rate sensitivity, rate-dependent damage and inertia of microcracking.

Acknowledgement

The authors acknowledge the financial support obtained from Gaz de France (GDF) and from Agence Nationale pour la Gestion des Déchets Radioactifs (ANDRA). Also, one of the authors, JRK, is grateful for the support of CNRS-France.

References

1. S. SERDENGECTI and G. D. BOOZER, *The effects of strain rate and temperature on the behavior of rocks subjected to triaxial compression*, p. 83, Proc. Fourth Symp. Rock Mech., Penn State 1961.
2. J. B. CHEATHAM, *The effect of pressure, temperature, and loading rate on the mechanical properties of rocks*, p. 388, in: Mechanical Behavior of Materials under Dynamic Loads, Springer, New York 1968.
3. K. O. HAKALEHTO, *The behaviour of rock under impulse loads*, Acta Polytechnica Scandinavica Ser. 81, Helsinki 1969.
4. U. S. LINDHOLM, L. M. YEAKLEY and A. NAGY, *The dynamic strength and fracture properties of Dressel basalt*, Int. J. Rock Mech. Min. Sci. and Geomech. Abstr., **11**, 181, 1974.
5. R. J. CHRISTENSEN, S. R. SWANSOW and W. S. BROWN, *Split Hopkinson bar test on rock under confining pressure*, Experim. Mech., **12**, 508, 1972.
6. R. D. PERKINS, S. J. GREEN and M. FRIEDMAN, *Uniaxial stress behaviour of porphyritic tonalite at strain rates to $10^3/s$*, Int. J. Rock Mech. Min. and Geomech. Abstr. Sci., **7**, 527, 1970.
7. D. E. GRADY and M. E. KIPP, *Oil shale fracture and fragmentation at high rates of loading*, p. 119, Proc. 20th U.S. Symposium Rock Mech., Austin, June 1979.
8. M. J. FORRESTAL, D. E. GRADY and K. W. SCHULER, *An experimental method to estimate the dynamic fracture strength of oil shale in the 10^3 to $10^4 s^{-1}$ strain rate regime*, Int. J. Rock Mech. Min. Sci. and Geomech. Abstr., **15**, 263, 1978.
9. H. KOLSKY, *An investigation of the mechanical properties of materials at very high rates of loading*, Proc. Phys. Soc. London, **B62**, 676, 1954.

10. E. D. H. DAVIES and S. C. HUNTER, *The dynamic compression testing of solids by the method of the split Hopkinson pressure bar*, J. Mech. Phys. Solids, **11**, 155, 1963.
11. J. Z. MALINOWSKI and J. R. KLEPACZKO, *A unified analytic and numerical approach to specimen behaviour in the split-Hopkinson pressure bar*, Int. J. Mech. Sci., **28**, 381, 1986.
12. P. BÉREST and D. MINH NGUYEN, *Deep underground storage cavities in rock salt*, p. 555, The Mechanical Behaviour of Salt, Proc. of the First Conference, Trans. Tech. Publ., Clausthal 1984.
13. J. R. KLEPACZKO, *Quasi-static and dynamic compression behaviour of coal*, Techn. Report, 1, 1982, Dept. of Mech. Engng. The Univ. of Manitoba, 1982.
14. J. R. KLEPACZKO, T. R. HSU and M. N. BASSIM, *Elastic and pseudo-viscous properties of coal under quasi-static and impact loadings*, Canadian Geotech. J., **21**, 203, 1984.
15. H. KOLSKY, *An investigation of the mechanical properties of materials at very high rates of loading*, Proc. Phys. Soc. London, **B62**, 676, 1949.
16. U. S. LINDHOLM, *Some experiments with the split Hopkinson pressure bar*, J. Mech. Phys. Solids, **12**, 317, 1964.
17. G. GARY and J. R. KLEPACZKO, *A complete computer program to analyse tension/compression test with the split Hopkinson bar*, Ecole Polytechnique, Palaiseau 1988.
18. J. R. KLEPACZKO, *Application of the modified split Hopkinson pressure bar for impact testing of rocks*, Engng. Trans., **20**, 1980.
19. J. R. KLEPACZKO, *The modified split Hopkinson bar*, Engng. Trans., **9**, 471, 1970.
20. B. LUNDBERG, *A split Hopkinson bar study of energy absorption in dynamic fragmentation*, Int. J. Rock Mech. Min. Sci and Geomech Abstr., **13**, 187, 1976.
21. N. L. CARTER and F. D. HANSES, *Creep of rock salt*, Technophysics, **92**, 275, 1983.
22. I. W. FARMER and M. J. GILBERT, *Time dependent strength reduction of rock salt*, The Mechanical Behaviour of Salt, Proc. of the First Cont., p. 3, Trans. Tech. Publ., Clausthal 1984.
23. M. E. KIPP, D. E. GRADY and E. P. CHEN, *Strain-rate dependent fracture initiation*, Int. J. Fract., **16**, 471, 1980.
24. J. R. KLEPACZKO, *On the role of microcracking inertia in rate sensitivity of coal at high strain rates*, Arch. Mech., **41**, 325, 1988.
25. W. JANACH, *The role of bulking in brittle failure of rocks under rapid compression*, Int. J. Mech. Min. Sci. and Geomech. Abstr., **13**, 177, 1976.
26. Z. MRÓZ and M. ANGELILLO, *Rate-dependent degradation model for concrete and rock*, p. 38, Proc. Inst. Symp. on Numerical Models in Geomechanics, Rotterdam 1982.
27. J. R. KLEPACZKO, *A general approach to rate sensitivity and constitutive modelling in FCC and BCC metals*, in: Impact: Effect of Fast Transient Loadings, p. 3, Rotterdam 1988..
28. U. F. KOCKS, A. S. ARGON and M. F. ASHBY, *Thermodynamics and kinetics of slip*, Pergamon Press, Oxford 1975.
29. J. R. KLEPACZKO, *Modelling of structural evolution at medium and high strain rates, FCC and BCC metals*, p. 387, Constitutive Relations and Their Physical Basis, Riso Natl. Laboratory, Roskilde 1987.
30. A. ARIELI, H. C. HEARD and A. K. MUKHERJEE, *Deformation modeling in sodium chloride at intermediate and elevated temperatures*, p. 342, Mechanical Testing for Deformation Model Develompent, ASTM STP 765, Philadelphia 1982.
31. H. F. FROST and M. F. ASHBY, *Deformation-mechanism maps*, Pergamon Press, Oxford 1982.
32. D. E. MUNSON and P. R. DAWSON, *Salt constitutive modeling using mechanism maps*, p. 717, The Mechanical Behavior of Salt Proc. of the First Conference, Trans. Tech. Publ., Clausthal 1984.
33. W. BLUM and C. FLEISCHMANN, *On the deformation-mechanism map of rock salt*, p. 7, The Mechanical Behavior of Salt, Proc. of the Second Conference, Trans. Tech. Publ., Clausthal 1988.
34. L. NEVILLE, L. CARTER and H. G. HEARD, *Temperature and rate dependent deformation of halite*, American J. Sci., **269**, 193, 1978.
35. J. E. RUSSEL, J. HANDIN and N. L. CARTER, *Modified mechanical equation of state for rock salt*, p. 409, The Mechanical Behavior of Salt, Proc. of the Second Conference, Trans. Tech. Publ., Clausthal 1988.
36. J. R. KLEPACZKO, *A power form of the mechanical equation of state with temperature*, Engng. Trans., **13**, 561, 1965.
37. J. R. KLEPACZKO, *A practical stress-strain-strain-rate-temperature constitutive equation of the power form*, J. Mech. Working Techn., **15**, 143, 1987.
38. U. HUNSCHE, *Private communication*, June 1989.

39. J. R. KLEPACZKO, *Behavior of rock-like materials at high strain rates in compression*, Int. J. of Plasticity, **6**, 415, 1990.
40. S. J. GREEN and R. D. PERKINS, *Uniaxial compression tests at strain rates frm* 10^{-4}*/sec to* 10^{4}*/sec on three geological materials*, p. 35, Proc. 10-th U.S. Symposium on Rock Mechanics 1968.
41. U. HUNSCHE, *On the fracture behavior of rock salt*, p. 18–1, Proc. 19th Canadian Fract. Conf., Ottawa 1989.
42. D. E. GRADY and M. E. KIPP, *The micromechanics of impact fracture of rock*, Int. J. Rock Mech. Sci and Geomech. Abstr., **16**, 293, 1979.
43. J. LANKFORD, *Inertia as a factor in the dynamic strength of brittle materials*, p. 232, Proc. Penn. State Conf., Pennsylvania 1981.

UNIVERSITE DE METZ, FAC. SCI.
LABORATOIRE DE PHYSIQUE ET MECANIQUE DES MATERIAUX, METZ,
AND
ECOLE POLYTECHNIQUE,
LABORATOIRE DE MECANIQUE DES SOLIDES, PALAISEAU, FRANCE.

Received March 8, 1991.